Anomalous birefringence in andradite–grossular solid solutions: a quantum-mechanical approach

Noname manuscript No.
(will be inserted by the editor)

Anomalous birefringence in andradite-grossular solid solutions

A quantum-mechanical approach

Valentina Lacivita · Philippe D'Arco · Roberto Orlando · Roberto Dovesi · Alessio Meyer

Received: June 19, 2013/ Accepted: –

Abstract The static linear optical properties (refractive indices, birefringence and axial angle) of andradite-grossular ($Ca_3Fe_2Si_3O_{12}$-$Ca_3Al_2Si_3O_{12}$) solid solutions have been computed at the *ab initio* quantum mechanical level through the Coupled Perturbed Kohn-Sham (CPKS) scheme, using an *all-electron* Gaussian-type basis set. Geometry relaxation after substitution of 1 to 8 Al for Fe atoms in the primitive cell of andradite yields 23 non-equivalent configurations ranging from cubic to triclinic symmetry. Refractive indices vary quite regularly between the andradite (1.860) and grossular (1.671) end-members; the birefringence δ and the axial angle $2V$ at intermediate compositions can be as large as 0.02 and 89°, respectively. Comparison with experiments suffers from inhomogeneities and impurities of natural samples; however, semi-quantitative agreement is observed.

Keywords garnets · solid solutions · grossular-andradite · anomalous birefringence · Coupled Perturbed Kohn-Sham · periodic calculations · gaussian basis set · CRYSTAL code

V. Lacivita
Dipartimento di Chimica, Università degli Studi di Torino
and NIS - Center of Excellence (http://www.nis.unito.it), Torino, Italy
Tel.: +39-011-6707560
E-mail: valentina.lacivita@unito.it

Ph. D'Arco
Institut des Sciences de la Terre de Paris (UMR 7193 UPMC-CNRS)
UPMC, Sorbonne Université, Paris, France

R. Orlando
Dipartimento di Chimica, Università degli Studi di Torino
and NIS - Center of Excellence (http://www.nis.unito.it), Torino, Italy

R. Dovesi
Dipartimento di Chimica, Università degli Studi di Torino
and NIS - Center of Excellence (http://www.nis.unito.it), Torino, Italy

A. Meyer
Dipartimento di Chimica, Università degli Studi di Torino
and NIS - Center of Excellence (http://www.nis.unito.it), Torino, Italy

1 Introduction

Garnets are silicates of general formula $X_3Y_2(SiO)_4$ and high symmetry (space group: cubic $Ia\bar{3}d$). Up to 12 pure members (*end-members*) have been recognized as belonging to this mineral group (Rickwood et al, 1968). *End-members* limit the range of composition for a number of complex solid solutions corresponding to different combinations of X^{2+} (Ca, Fe, Mg, Mn) and/or Y^{3+} (Al, Fe, Cr) cations.

Garnet solid solutions apparently retain a cubic metric but often show optical anisotropy. Several examples of this *anomalous* behaviour have been studied, dealing either with optical anisotropy in structurally *isometric* garnets (Foord and Mills, 1978) or with the presence of two optical axes in formally uniaxal crystals (Kahr and McBride, 1992). The origin of such a phenomenon has been extensively discussed since the nineteenth century (Brewster, 1853; Mallard, 1876), but still remains controversial (Shtukenberg et al, 2001).

Strain can account for anomalous anisotropy. Hypotheses on the origin of such stress-induced birefringence refer (a) to the application of mechanical stress or (b) to large compositional changes between growth *striae* that produce lattice mismatches in (rythmically or not) chemically zoned crystals (Lessing and Standish, 1973; Kitamura and Komatsu, 1978). In case (a), it is believed that annealing treatments at relatively low-temperature can cancel this anomalous behaviour (Allen and Buseck, 1988; Hofmeister et al, 1998). Other hypotheses regard non-cubic distributions of OH groups after hydrogarnet substitution (Rossman and Aines, 1986) or the replacement of Ca with Rare Earth Elements (REE) (Blanc and Maisonneuve, 1973). The following discussion will focus on unstrained garnets.

Optical anisotropy is quite common in (if not limited to) Ca-rich garnets (McAloon and Hofmeister, 1995) from contact metamorphic calcareous rocks, rapidly grown from magmatic fluids. Such garnets are chemically zoned and display twinning-like sectoring superimposed to growth-related chemical variations (Jamtveit and Andersen, 1992). Andradite and grossular (*grandite*) components usually account for more than 90% of their composition. On the contrary, Ca-poor garnets grown from regional metamorphic rocks - in which crystallization is a much slower process - rarely show optical anisotropy. Hofmeister et al (1998) have analyzed a series of 47 Ca-poor garnets displaying wavy (or ondulatory) optical properties and very weak birefringence which, they concluded, were mostly due to mechanical stress. The foregoing suggests that kinetics could play a significant role in the formation of anisotropic Ca-rich garnets.

X-ray diffraction (XRD) structure refinements carried out until 1982 failed to identify non cubic symmetries in anisotropic garnets. To our knowledge, Takeuchi et al (1982) were the first to report cases of orthorhombic and monoclinic structures obtained for carefully selected fragments of *quasi* binary andradite-grossular samples from three different places. Since then, only a few other structure refinements (Andrut and Wildner, 2001; Wildner and Andrut, 2001; Shtukenberg et al, 2002) yielded non-cubic (but orthorhombic, monoclinic or triclinic) Ca-rich garnets with very weak unit cell distorsions, usually characterized by some cation ordering in Y sites. Thus, birefringence in these compounds may be explained with a lowering of symmetry due to a certain selectivity at the Y sites (a microscopic, fully random distribution of the substituted atoms would lead to a macroscopic restoration of the original symmetry, and birefringence would be eliminated). This ordering may have either a thermodynamic (Hofmeister et al, 1998; Akizuki, 1984) or a kinetic origin (Allen and Buseck, 1988; Andrut and Wildner, 2001; Wildner and Andrut, 2001; Shtukenberg et al, 2002).

Thermodynamics would play a role as the difference in size and electronic properties of trivalent cations (e.g. Fe^{3+} and Al^{3+}) is supposed to drive ordering and thus introduce sig-

nificant deviations from ideal isotropic optical behavior. However, despite some differences, both experimental (Engi and Wersin, 1987) and numerical data (Becker and Pollok, 2002) suggest that atom ordering requires low temperatures (770 K Engi and Wersin (1987) or 500 K (Becker and Pollok, 2002)) at which the sluggish cation diffusion would not produce any measurable effect even on geological time scales.

In the second case, the symmetry lowering from cubic conditions could be attributed to the *growth mechanism* (Allen and Buseck, 1988; Akizuki, 1984; Gali, 1983). Desymmetrization would result from the fact that, during growth, symmetry equivalences between crystal faces may be lost, thus inducing differential chemical selectivity within the *Y* sites and yielding progressive sectoring, easily observable by optical microscopy.

A major argument in favor of a kinetic origin of anomalous birefringence in garnets settles on its large variability for a given composition. Mariko and Nagai (1980) describe three andradite-grossular garnets distinguished on the basis of their occurrence and composition. One group includes isotropic garnets with 28% to 67% of andradite (A); a second group includes optically *anomalous* garnets in which the andradite percentage ranges from 46% to 100% (B1); finally, a third group (B2) includes garnets with the same chemical composition as those in A but showing optical anisotropy as those in B1. For both series B1 and B2, the dependence of the birefringence δ on the chemical composition is shown. As a general trend, δ tends to zero at the extremes (i.e. end-members) and reaches its maxima at intermediate compositions, the particular values being substantially different between the B1 group and the B2 one: δ can be as large as 0.01 in B1, but only 0.004 in B2. That is, within a common domain of compositions, *anomalous* garnets display large differences in birefringence (up to about one order of magnitude, as recorded in Ref. Mariko and Nagai 1980), which supports the role of crystallization conditions in determining different degrees of order.

In simulation, we cannot tackle directly the whole complexity of this issue, but rather select some ideal fully ordered compositional configurations with a given symmetry. Their birefringence would be representative of the upper limit expected for the birefringence of Ca-rich garnets, as opposed to the isotropic fully random case.

As a further step with respect to previous theoretical semi-classical works (Shtukenberg et al, 2002), we cut empirical dependencies by adopting a quantum-mechanic *ab initio* approach and making reference to well defined configurations of the primitive cell. Variational solutions to the Shrödinger equation have been obtained with the first-principle all-electron Gaussian-based code CRYSTAL (Dovesi et al, 2009) for simulations on periodic systems. To the authors' knowledge, this is the first theoretical *ab initio* work addressed to such a systematic analysis. The related goal is accessing the geometrical distorsion from cubic symmetry induced by ordering of the octahedral independent cations (how large is it?). This can shed light on the reason why only very few non-cubic structures have been detected during X-ray analyses on natural garnets.

Structure and thermodynamic properties of *grandite* solid solutions have already been investigated by some of the present authors (De La Pierre et al, 2013). We apply here the Coupled Perturbed (CP) Hartree-Fock/Kohn-Sham (HF/KS) scheme (Hurst et al, 1988), generalized to periodic systems (Kudin and Scuseria, 2000; Kirtman et al, 2000) and recently implemented in CRYSTAL (Ferrero et al, 2008a,c,b,d), to compute analytical static dielectric constants and related linear optical properties (refractive indices, birefringence and axial angle).

2 Method

2.1 Coupled-Perturbed Hartree-Fock

Analytical formulae for estimating the energy derivatives with respect to a static uniform electric field ε are provided by the CPHF method (Hurst et al, 1988) implemented in a local variational basis within the CRYSTAL code (Dovesi et al, 2009).

Basically, the scheme focuses on the description of the relaxation of Crystalline Orbitals (CO)

$$\Psi_i(\mathbf{r},\mathbf{k}) = \sum_{\mu} \psi_{\mu}(\mathbf{r},\mathbf{k}) C^{\mathbf{k}}_{\mu i} \tag{1}$$

i.e. linear combinations of Bloch Functions (BF) $\psi_{\mu}(\mathbf{r},\mathbf{k})$ - under the effect of an electric field. As the variational freedom lies in coefficients $C^{\mathbf{k}}_{\mu i}$ of Eq. (1), they cope with the applied perturbation through the unitary transformation

$$\frac{\partial C^{\mathbf{k}}_{\nu j}}{\partial \varepsilon_t} \equiv C^{\mathbf{k},t}_{\nu j} = \sum_{j} C^{\mathbf{k}}_{\mu i} \mathsf{U}^{\mathbf{k},t}_{ij} \tag{2}$$

CRYSTAL provides a Self-Consistent (SC) solution to Eq. (2) by exploiting the equality

$$\mathsf{U}^{\mathbf{k},t}_{ij} = \frac{F^{\mathbf{k},t}_{ij}}{E_j - E_i} \tag{3}$$

which involves the difference between the unperturbed eigenvalues E_i and E_j, and the derivative of the Fock matrix with respect to the tth field component, $F^{\mathbf{k},t}_{ij}$, in turn depending on $\mathsf{U}^{\mathbf{k},t}$ through the density matrix.
Convergence is monitored on the variation of the energy second derivative

$$\frac{\partial^2 E_{tot}}{\partial \varepsilon_t \partial \varepsilon_u} = -\frac{2}{n_k} \Re \left(P_{t,u} \sum_{\mathbf{k}}^{BZ} \sum_{j}^{occ} \sum_{l}^{virt} \Omega^{\mathbf{k},t}_{jl} \mathsf{U}^{\mathbf{k},u}_{lj} \right) \tag{4}$$

where n_k is the number of $\mathbf{k}$ points in the first Brillouin zone; $\Re$ selects the real part of the expression in parentheses; $P_{t,u}$ exchanges the field components t and u and $\Omega^{\mathbf{k},t}_{ij}$ is the component t of the perturbation operator (Kudin and Scuseria, 2000; Kirtman et al, 2000; Otto, 1992; Otto et al, 1999; Izmaylov et al, 2006; Springborg and Kirtman, 2007)

$$\hat{\Omega}(\mathbf{k}) = e^{\imath \mathbf{k}\cdot\mathbf{r}} \nabla_{\mathbf{k}}\, e^{-\imath \mathbf{k}\cdot\mathbf{r}} \tag{5}$$

represented in the unperturbed CO basis.

Equation (4) defines the static polarizability α_{tu} (Bohr^3) per unit cell (of volume V), which is related to the macroscopic dielectric constant ε_{tu} as

$$\varepsilon_{tu} = \frac{4\pi}{V} \alpha_{tu} + \delta_{tu} \tag{6}$$

Once the whole dielectric tensor ε has been calculated, it is diagonalized to provide the principal refractive indices as square roots of its eigenvalues.

2.2 Selected cation distributions

Reference has been made to the ideal cubic structure of andradite, $Ca_3Fe_2Si_3O_{12}$ (And). Its primitive cell contains 80 atoms, 8 of which are Fe^{3+} cations ($n_{Fe} = 8$) arranged in as many equivalent octahedral *Y* sites. *Solid solutions* were obtained by progressively replacing Fe^{3+} ions with a number n_{Al} of Al^{3+} atoms, up to grossular, $Ca_3Al_2Si_3O_{12}$ (Gro). For each composition $x = \frac{n_{Al}}{n_{Al}+n_{Fe}}$ there exist $\frac{8!}{x!(8-x)!}$ geometrical configurations grouped into symmetry equivalent classes L, with N_L residual symmetry operators.

According to the symmetry analysis carried out by Mustapha *et al.* (Mustapha et al, 2013), the And-Gro series counts for 23 classes of degenerate configurations, as many as the geometry full optimizations that were performed out of the full set of 256 substitutional configurations, with a significant reduction of the computational cost. Only the highest spin ferromagnetic configurations have been considered, as the difference between ferromagnetic (FM) and anti-ferromagnetic (AFM) energies was shown to be extremely small (Meyer et al, 2010) and the birefringence is almost independent of the spin configuration (see below). Structural and thermodynamic details have been addressed to in a previous work (De La Pierre et al, 2013).

2.3 Computational details

All calculations have been performed with a development version of the CRYSTAL code (Dovesi et al, 2009). The valence open-shell of Fe^{3+}, d^5, requires a spin-polarized solution. In order to provide accurate description of unpaired *d* electrons localized on transition metal ions, the B3LYP (Becke, 1993; Lee et al, 1988) hybrid mixing of nonlocal Density Functional (DF) correlation and HF exchange has been adopted confidently (Moreira et al, 2002; Moreira and Dovesi, 2004; Zicovich Wilson et al, 2004; Prencipe et al, 2004; Pascale et al, 2005b,a; Orlando et al, 2006; Zicovich Wilson et al, 2008; Patterson, 2008; Meyer et al, 2010; Lacivita et al, 2009).

An all electron basis set was used for all atoms. Oxygen, silicon, calcium, aluminum and iron are described by (8s)(411sp)(1d), (8s)(6311sp)(1d), (8s)(6511sp)(1d), (8s)(611sp)(21d) and (8s)(64111sp)(411d)(1f) contractions, respectively. Beyond geometry optimizations - for which effectiveness of such basis set has been already proven (Pascale et al, 2005a,b; Zicovich Wilson et al, 2008; Meyer et al, 2010), a previous study (Meyer et al, 2009) has shown that it performs properly also in the calculation of the polarizabilities.

Convergence of the Self-Consistent-Field (SCF) on the total energy was set to $\Delta E = 10^{-7}$ Ha and the Monkhorst net has been generated by using a shrinking factor $S = 2$, which samples from 3 to 8 **k** points of the first Brilluin zone, depending on whether the configuration symmetry is maximum (cubic cell) or minimum (triclinic cell). A grid of extra-large size was used for integration of the exchange-correlation density functional and tolerances for the truncation of the infinite Coulomb and exchange sums were set to $T_1 = T_2 = T_3 = 7$ and $T_4 = \frac{1}{2}T_5 = 8$, see the CRYSTAL manual (Dovesi et al, 2009) for explanation.

The structures have been optimized using analytical energy gradients with respect to both atomic coordinates and lattice parameters (Doll, 2001; Doll et al, 2001; Civalleri et al, 2001), with a quasi-Newton scheme combined with the BFGS algorithm for Hessian updating (Broyden, 1970; Fletcher, 1970; Goldfarb, 1970; Shanno, 1970). Convergence to equilibrium has been checked on both gradient components and nuclear displacements, for which the default threshold values are chosen (Dovesi et al, 2009).

3 Results and discussion

3.1 Structure

Details on the structural data obtained from B3LYP geometry optimizations are reported in Ref. (De La Pierre et al, 2013). The cell parameter decreases linearly along the series of compositions, from 12.19 Å of And to 11.96 Å of Gro. A slight overestimation of the experimental data on the end-members structures, i.e. 12.06 Å (Armbruster and Geiger, 1993) and 11.84 Å (Mittal et al, 2001), meets expectations on the performance of the B3LYP hybrid functional (Paier et al, 2007).

Differences in size and electronic configuration between Al^{3+} and Fe^{3+} induce geometrical distorsions in *grandite* solid solutions with respect to the original cubic structure. Yet, all the calculated cells are pseudocubic: cell edges differ by less than 0.01 Å and angles by less than 0.4° (from 90°), in good agreement with the values of 0.006 Å and 0.12° reported as the largest geometrical distorsion encountered by Shtukenberg et al (2002) (and Refs. therein) in non cubic *grandite* garnets. This may be at the origin of birefringence of solid solutions, departing weakly from cubic metric but significantly from cubic symmetry. A quantitative discussion on this point is the subject of the next paragraph.

3.2 Optical observations

Table 1 reports the main refractive indices $\alpha \leq \beta \leq \gamma$, the birefringence $\delta = \gamma - \alpha$ and the optical $2V$ angle calculated for the 23 classes of configurations analyzed along the And-Gro binary.

The refractive indices computed for the end-members, namely 1.860 for And and 1.671 for Gro, deviate by less than 3% from experiment (Medenbach and Shannon, 1997). The evolution of α, β and γ indices is represented in Figure 1 through their average value n_{av} per class L. A linear decrease of n_{av} *vs* x can be observed, that is of the order of 2-3 cents per Y site substitution. The simultaneous lowering of the density from 3.720 g/cm^3 of And to 3.492 g/cm^3 of Gro justifies such a descending trend (Marler, 1988). On the other hand, polymorphic classes - i.e. symmetry independent classes for a given composition - all exhibit very similar $n_{av}(x\%)$. Comparison with experimental values is a delicate issue because of their frequency dependence. The available experimental data have been split into two main sets: Exp. A and Exp. B corresponding, respectively, to anisotropic and isotropic garnets. Set Exp. C only includes the *end-member* indices extrapolated at infinite wave-length (Medenbach and Shannon, 1997). A least squares best fitting yields $s_{AB} = -0.0015$ as a slope for the interpolating line. Sample impurities, such as minor portions of end-member garnets other than the strictly And-Gro binary (e.g. almandine, spessartine, uvarovite, pyrope) may account for data dispersion in sets A and B. The calculated values are affected by a slight but systematic underestimation (about 3%), for less than a little divergence for grossular-rich solutions ($s_{calc} = -0.0019$). However, further comparison with the linear *ideal* pattern connecting values $n_{av}(0) = 1.832 - 1.835$ and $n_{av}(100) = 1.717 - 1.723$ from set Exp. C (slope $s_C = -0.0011$) highlights a relatively large range of uncertainty on the experimental data.

Figure 2 compares observed (McAloon and Hofmeister, 1995; Mariko and Nagai, 1980) (solid dots) and calculated (circles) birefringence for each class of configurations at composition x. For pseudo-cubic configurations our theoretical treatment yields non zero though weak birefringence δ: the upper limit is of order 0.02. Differences between polymorphic

configurations are pretty small. Almost all the experimental data lie below the upper limit here estimated for δ. Only the birefringence of classes $L = 11$ and $L = 12$ lies within the range of experimental values, but these configurations are among the least probable at the temperatures of formation (De La Pierre et al, 2013). If we consider the general trend of the birefringence δ, which grows at intermediate compositions ($x = 50\%$) and decreases towards the end-members ($x \to 0$ and $x \to 100\%$), the agreement with experiments may be considered as satisfactory.

Let us refer to the sum of the squared differences between the right angle (90°) and the angles of a pseudo-cubic cell as a quantitative estimate of the corresponding geometric distortion, $\Theta = \sum_i (90 - \theta_i)^2$. We may define a distortion data set for the 23 *grandite* configurations using the structure parameters reported by De La Pierre et al (2013). The plot of δ *versus* Θ - Figure 3 - provides a linear correlation coefficient $r = 0.903$, indicating that about 82% of variation is shared between the birefringence and the geometric distortion. Different symbols in Figure 3 correspond to different compositions. It is noteworthy that each set of points at a given composition roughly obeys the same trend: δ is more or less constant within a certain deformation range; then, as Θ increases, the birefringence increases. This supports our analysis of the correlation coefficient.

We also tested the importance of the spin configuration with respect to the onset of birefringence, considering the simple case where all but two Fe atoms are replaced by Al in the Y sites ($x = 0.75$, $L = 19, 20, 21$). As the magnetic interactions between second and farther neighbors is negligible (Meyer et al, 2010), we can rule out the $20th$ class and focus on classes 19 and 21 where the transition metal ions are nearest neighbors at 5.1756 and 5.2108 Å, respectively. By comparison between the minimum energy difference between these two geometric configurations (> 2000 μHa) and the energy lowering associated with antiferromagnetism (100-200 μHa) (Meyer et al, 2010) we expect little influence of magnetic interactions on the calculated optical properties. This is actually the case, the calculated birefringence for FM and AFM spin configurations differing by less than 4% in the worst case, *i.e.* $\delta = 0.0128$ (FM) *vs.* $\delta = 0.0133$ (AFM) for $L = 21$, which is not even one tenth of the δ variation related to the increased symmetry at $L = 19$. Spin effects can then be safely neglected.

In Table 1, we distinguish among positive and negative configurations using the optical angle $(\pm)2V$ (in degrees), being $2V = 0$ for uniaxial configurations and $2V \neq 0$ for biaxial configurations (column 3, Table 1). Each compositional class includes at least one uniaxial configuration (of trigonal or tetragonal symmetry) with opposite sign in complementary And-like and Gro-like compositions. Biaxial configurations generally correspond to large optical angles: the lowest limit is about 60°. Our $2V$ angles are in good agreement with theoretical values obtained by Shtukenberg *et al.* (Shtukenberg et al, 2002). They applied the point-dipole model to determine the *anomalous* optical indicatrices of four And-Gro crystals comprising from about 40% to 80% of Gro. They report also the optical angle $2V = 80(5)^\circ$ observed (Shtukenberg et al, 2001) for the Mali garnet $Ca_3(Fe_{0.23}Al_{0.77})_2(SiO_4)_3$, which overlaps perfectly to the angles here estimated for monoclinic configurations of composition $Ca_3(Fe_{0.25}Al_{0.75})_2(SiO_4)_3$ (n_{Al} = 6 in Table 1), i.e. 77° and 88°. The same applies to the optical angle $2V = (+)80^\circ$ observed by Akizuki (Akizuki, 1984) on a specimen from Eden Hill (Vermont) of chemical composition $Gro_{85.7}And_{14.3}$.

4 Conclusions

The *anomalous* optical anisotropy of grossular-andradite solid solutions has been investigated by using *ab initio* simulation. Substitutions over the octahedral sites of a unit cell volume give rise to 23 symmetry-independent classes of configurations. By structural relaxation, such configurations undergo small distorsions from the cubic metric (i.e. cell parameters $a = b = c$ and angles $\alpha = \beta = \gamma = 90°$), not exceeding however a hundreth of Å and a tenth of a degree, respectively. These distorsions compare well with the few experimental data available. As expected, calculating the birefringence of a unit cell substituted at the Y-sites draws an upper limit for the dispersion of the observed *anomalous* birefringence, the latter being *per se* in wide variability for similar compositions (Mariko and Nagai, 1980). The perfect periodicity of our theoretical model suggests that (partial) kinetic ordering may account for optical anisotropy in real samples. The calculated average refractive index n_{av} reproduces the experimental descending trend with the composition And ($x_{Al} = 0$) $\rightarrow$ Gro ($x_{Al} = 1$), except for a slight but systematic underestimation. Likewise, our results on optical angles of biaxial configurations compare well with measured data.

Table 1 The linear optical properties of *grandite* solid solutions. n_{Al} is the number of Al atoms substituted for Fe in the octahedral Y sites. L labels the symmetry independent configurations. *Sym* indicates the crystal system of the primitive cell, attributed on the basis of the symmetry operators. α, β and γ are the principal refractive indices, being $\alpha \leq \beta \leq \gamma$. $\delta = \gamma - \alpha$ (adimensional) is the birefringence; $(\pm)2V$ (in degrees) is the optic angle ($2V = 0$ for uniaxial configurations) whose sign is used to distinguish between positive and negative configurations.

n_{Al}	L	*Sym*	$2V$	α	β	γ	δ
0	1	cub		1.860			
1	2	trig	$(+)0$	1.834	1.841		0.007
	3	trig	$(+)0$	1.807	1.823		0.016
2	4	mon	$(+)71$	1.809	1.812	1.819	0.010
	5	mon	$(-)89$	1.808	1.813	1.818	0.010
	6	trig	$(-)0$	1.786	1.793		0.008
3	7	tric	$(+)68$	1.781	1.786	1.799	0.018
	8	tric	$(-)67$	1.784	1.791	1.794	0.009
	9	cub		1.768			
	10	ort	$(+)77$	1.754	1.763	1.777	0.023
	11	tet	$(-)0$	1.764	1.768		0.004
4	12	trig	$(+)0$	1.766	1.767		0.001
	13	mon	$(-)80$	1.757	1.766	1.773	0.016
	14	mon	$(+)58$	1.759	1.762	1.775	0.016
	15	tric	$(+)85$	1.758	1.765	1.774	0.016
	16	trig	$(+)0$	1.740	1.750		0.010
5	17	tric	$(-)84$	1.732	1.742	1.751	0.019
	18	tric	$(+)59$	1.738	1.741	1.748	0.010
	19	trig	$(-)0$	1.705	1.724		0.019
6	20	mon	$(+)77$	1.713	1.718	1.726	0.013
	21	mon	$(-)88$	1.712	1.719	1.725	0.013
7	22	trig	$(-)0$	1.688	1.698		0.010
8	23	cub		1.671			

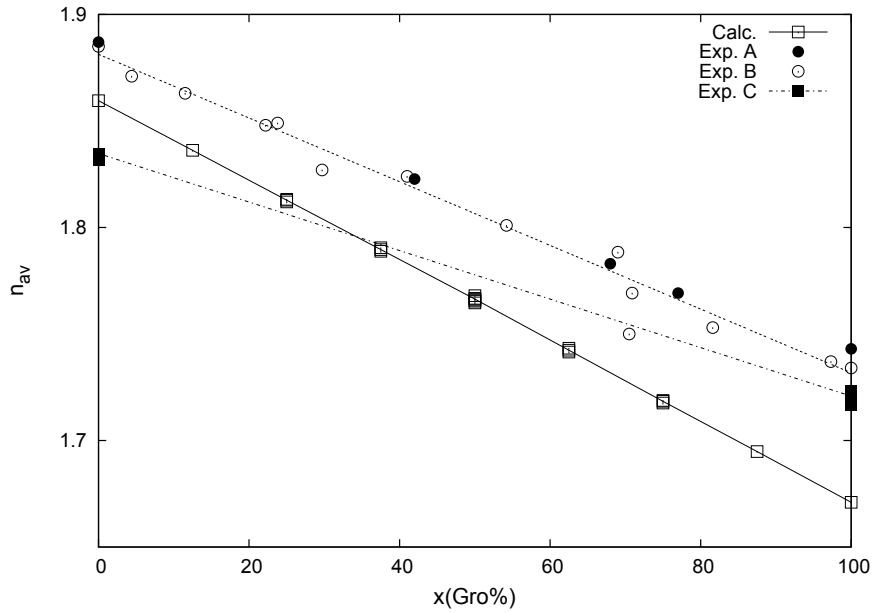

Fig. 1 Comparison between calculated average (Calc.) and experimental (Exp.) refractive indices for andradite-grossular binary. Calculated values (squares) refer to the mean refractive index, n_{av}, obtained for each configuration L. The standard deviation lies within the area enclosed by each square. Sets Exp. A (Shtukenberg et al, 2002) and Exp. B (Shtukenberg et al, 2002; Deer et al, 1997) include experimental data on anisotropic and isotropic garnets, respectively. Set Exp. C (Medenbach and Shannon, 1997) shows the end-members indices extrapolated at $\lambda = \infty$. Straight lines are obtained by best fitting, the slopes being $s_{AB} = -0.0015$, $s_C = -0.0011$ and $s_{Calc} = -0.0019$.

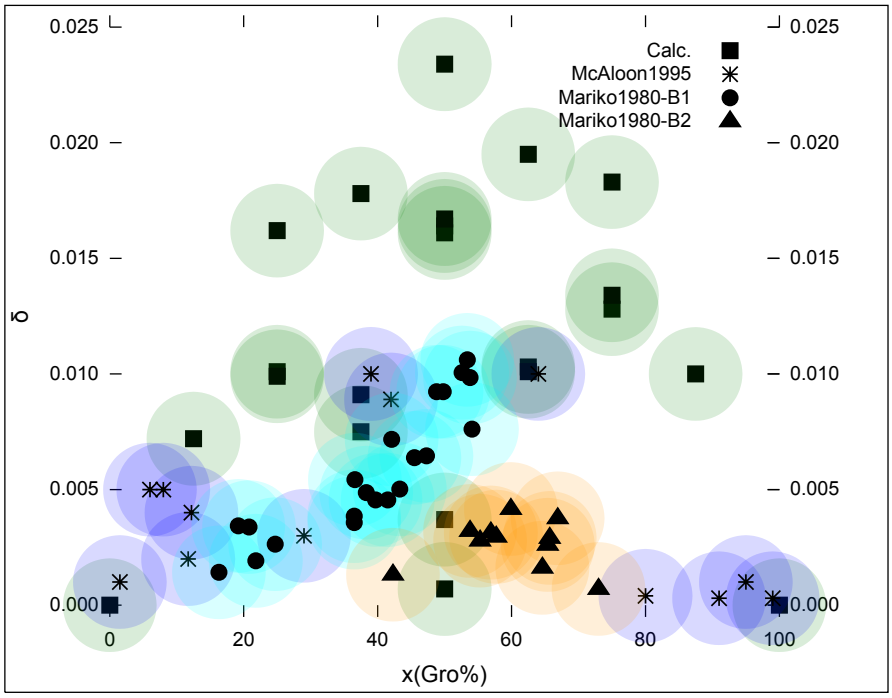

Fig. 2 Representation of birefringence δ *versus* composition $x(\%) = Al/(Al+Fe)$ of the andradite-grossular binary varies from $x = 0$ (And) to $x = 100$ (Gro). Comparison with experimental data from Refs. (McAloon and Hofmeister, 1995; Mariko and Nagai, 1980) is made.

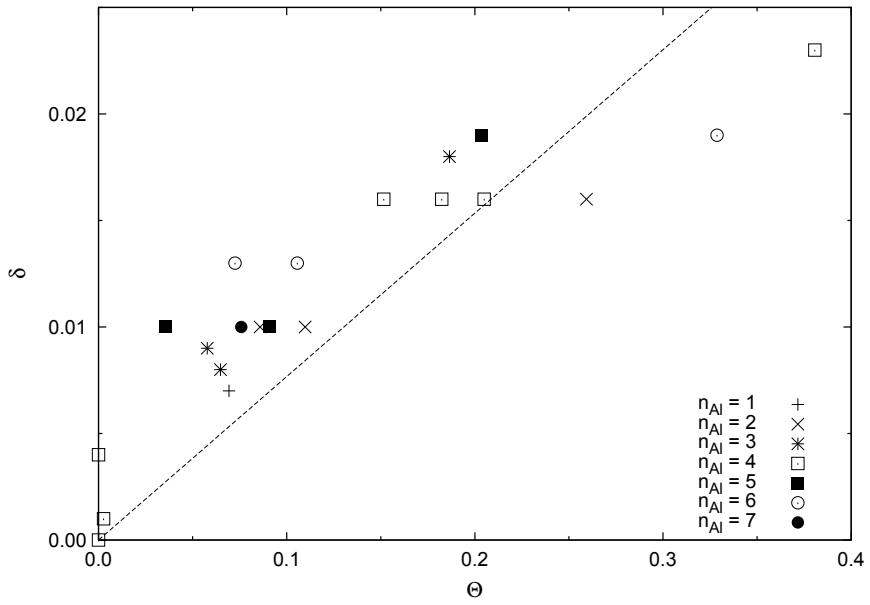

Fig. 3 Plot of the birefringence δ (adimensional) *versus* the structure distortion Θ (in squared degrees) associated to the 23 configurations (see text for definitions). Different symbols correspond to different compositions, *i.e.* different numbers of Al atoms substituted for Fe, n_{Al}.

References

Akizuki M (1984) Origin of optical variations in grossular-andradite garnet. Am Mineral 69:328

Allen FM, Buseck PR (1988) XRD, FTIR, and TEM studies of optically anisotropic grossular garnets. Am Mineral 73:568

Andrut M, Wildner M (2001) The crystal chemistry of birefringent natural uvarovites. Part III. Application of the superposition model of crystal fields with a characterization of synthetic cubic uvarovite. Am Mineral 86:1219

Armbruster T, Geiger CA (1993) Andradite crystal chemistry, dynamic X-site disorder and strain in silicate garnets. Eur J Mineral 5:59

Becke AD (1993) Density-functional thermochemistry. III. The role of exact exchange. J Chem Phys 98:5648

Becker U, Pollok K (2002) Molecular simulations of interfacial and thermodynamic mixing properties of grossular-andradite garnets. Phys Chem Miner 29:52

Blanc Y, Maisonneuve J (1973) Sur la biréfringence des grenats calciques. B Soc Fr Mineral Cr 96:320

Brewster D (1853) Phil Mag Ser 4 6:371

Broyden CG (1970) The Convergence of a Class of Double-rank Minimization Algorithms 1. General Considerations. J Inst Math Appl 6:76

Civalleri B, D'Arco Ph, Orlando R, Saunders VR, Dovesi R (2001) Hartree-Fock geometry optimization of periodic system with the CRYSTAL code. Chem Phys Lett 348:131

De La Pierre M, Noel Y, Mustapha S, Meyer A, D'Arco Ph, Dovesi R (2013) The infrared vibrational spectrum of andradite-grossular solid solutions. A quantum-mechanical simulation. Am Mineral 98:966

Deer WA, Howie RA, Zussman J (1997) Orthosilicates. Rock-Forming Minerals, Geological Society

Doll K (2001) Implementation of analytical Hartree-Fock gradients for periodic systems. Comput Phys Commun 137:74

Doll K, Harrison NM, Saunders VR (2001) Analytical Hartree-Fock gradients for periodic systems. Int J Quant Chem 82:1

Dovesi R, Saunders VR, Roetti C, Orlando R, Zicovich Wilson CM, Pascale F, Doll K, Harrison NM, Civalleri B, Bush IJ, D'Arco Ph, Llunell M (2009) CRYSTAL09 User's Manual. Università di Torino, Torino

Engi M, Wersin P (1987) Derivation and application of a solution model for calcic garnet. Schweiz Mineral Petrogr Mitt 67:53

Ferrero M, Rérat M, Kirtman B, Dovesi R (2008a) Calculation of first and second static hyperpolarizabilities of one- to three-dimensional periodic compounds. Implementation in the CRYSTAL code. J Chem Phys 129:244110

Ferrero M, Rérat M, Orlando R, Dovesi R (2008b) Coupled perturbed Hartree-Fock for periodic systems: the role of symmetry and related computational aspects. J Chem Phys 128:014110

Ferrero M, Rérat M, Orlando R, Dovesi R (2008c) The calculation of static polarizabilities of periodic compounds. The implementation in the CRYSTAL code for 1D, 2D and 3D systems. J Comput Chem 29:1450

Ferrero M, Rérat M, Orlando R, Dovesi R, Bush I (2008d) Coupled Perturbed Kohn-Sham calculation of static polarizabilities of periodic compound. J Phys Conf Ser 117:12016

Fletcher R (1970) A new approach to variable metric algorithms. Comput J 13:317

Foord EE, Mills BA (1978) Biaxiality in 'isometric' and 'dimetric' crystals. Am Mineral

63:316
Gali S (1983) Grandite garnet structures in connection with the growth mechanism. Z Kristallogr 163:43
Goldfarb D (1970) A Family of Variable-Metric Methods Derived by Variational Means. Math Comput 24:23
Hofmeister AM, Schaal RB, Campbell KM, Berry SL, Fagan TJ (1998) Prevalence and origin of birefringence in 48 garnets from pyrope-almandine-grossularite-spessartine quaternary. Am Mineral 83:1293
Hurst GJB, Dupuis M, Clementi E (1988) Ab initio analytic polarizability, first and second hyperpolarizabilities of large conjugated organic molecules: Applications to polyenes C_4H_6 to $C_{22}H_{24}$. J Chem Phys 89:385
Izmaylov AF, Brothers EN, Scuseria GE (2006) Linear-scaling calculation of static and dynamic polarizabilities in Hartree-Fock and density functional theory for periodic systems. J Chem Phys 125:224105
Jamtveit B, Andersen TB (1992) Morphological instabilities during rapid growth of metamorphic garnets. Phys Chem Miner 19:176
Kahr B, McBride JM (1992) Optically Anomalous Crystals. Angew Chem Int Edit 31:1
Kirtman B, Gu FL, Bishop DM (2000) Extension of the Genkin and Mednis treatment for dynamic polarizabilities and hyperpolarizabilities of infinite periodic systems. I. Coupled perturbed Hartree-Fock theory. J Chem Phys 113:1294
Kitamura K, Komatsu H (1978) Optical anisotropy associated gowth striation of yttrium garnet, $Y_3(Al,Fe)O_{12}$. Krist Tech 13:811
Kudin KN, Scuseria GE (2000) An efficient finite field approach for calculating static electric polarizabilities of periodic systems. J Chem Phys 113:7779
Lacivita V, Rérat M, Kirtman B, Ferrero M, Orlando R, Dovesi R (2009) Calculation of the dielectric constant ε and first nonlinear susceptibility $\chi^{(2)}$ of crystalline potassium dihydrogen phosphate by the coupled perturbed Hartree-Fock and coupled perturbed Kohn-Sham schemes as implemented in the CRYSTAL code. J Chem Phys 131:204509
Lee C, Yang W, Parr RG (1988) Development of the Colle-Salvetti correlation-energy formula into a functional of the electron density. Phys Rev B 37:785
Lessing P, Standish RP (1973) Zoned garnet from Crested Butte, Colorado. Am Mineral 58:840
Mallard E (1876) Ann Mines Mem VII Ser 10:60
Mariko T, Nagai Y (1980) Birefringence and composition of grandite garnet from the Shinyama ore deposit of the Kamaishi mine, Iwate Prefecture, Japan. Mineral J 10:181
Marler B (1988) On the Relationship between Refractive Index and Density for SiO_2-polymorphs. Phys Chem Miner 16:286
McAloon BP, Hofmeister AM (1995) Single-crystal IR spettroscopy of grossular-andradite garnets. Am Mineral 80:1145
Medenbach O, Shannon RD (1997) Refractive indices and optical dispersion of 103 synthetic and mineral oxides and silicates measured by a small-prism technique. J Opt Soc Am B 14:3299
Meyer A, Ferrero M, Valenzano L, Zicovich Wilson CM, Orlando R, Dovesi R (2009) Coupled Perturbed HF/KS calculation of the dielectric constant of crystalline systems. The case of six members of the garnet family. In: International Conference of Computational Methods in Sciences and Engineering 2009. Special Symposium in Honour of Professor Bernard Kirtman, B. Champagne and F. L. Gu and J. M. Luis and M. Springborg, Hotel Rodos Palace, Rhodes, Greece, pp 54–57
Meyer A, Pascale F, Zicovich Wilson CM, Dovesi R (2010) Magnetic interactions and elec-

tronic structure of uvarovite and andradite garnets. An ab initio all-electron simulation with the CRYSTAL06 program. Int J Quant Chem 110:338

Mittal R, Chaplot S, Choundry N (2001) Lattice dynamics calculations of the phonon spectra and thermodynamic properties of the aluminosilicate garnets pyrope, grossular, and spessartine $M_3Al_2Si_3O_{12}$ (M=Mg, Ca, and Mn). Phys Rev B 64:094302

Moreira IdePR, Dovesi R (2004) Periodic approach to the electronic structure and magnetic coupling in $KCuF_3$, K_2CuF_4, and $Sr_2CuO_2Cl_2$ low-dimensional magnetic systems. Int J Quant Chem 99:805

Moreira IdePR, Illas F, Martin RL (2002) Effect of Fock exchange on the electronic structure and magnetic coupling in NiO. Phys Rev B 65:155102

Mustapha S, D'Arco Ph, De La Pierre M, Noel Y, Ferrabone M, Dovesi R (2013) On the use of symmetry in configurational analysis for the simulation of disordered solids. J Phys: Condens Matter 25:105401

Orlando R, Torres FJ, Pascale F, Ugliengo P, Zicovich Wilson C, Dovesi R (2006) Vibrational spectrum of katoite $Ca_3Al_2[(OH)_4]_3$: a periodic ab initio study. J Phys Chem B 110:692

Otto P (1992) Calculation of the polarizability and hyperpolarizabilities of periodic quasi-one-dimensional systems. Phys Rev B 45:10876

Otto P, Gu FL, Ladik J (1999) Calculation of ab initio dynamic hyperpolarizabilities of polymers. J Chem Phys 110:2717

Paier J, Marsman M, Kresse G (2007) Why does the B3LYP hybrid functional fail for metals? J Chem Phys 127:024103

Pascale F, Catti M, Damin A, Orlando R, Saunders VR, Dovesi R (2005a) Vibration frequencies of $Ca_3Fe_2Si_3O_{12}$ andradite: an ab initio study with the CRYSTAL code. J Phys Chem B 109:18522

Pascale F, Zicovich Wilson CM, Orlando R, Roetti C, Ugliengo P, Dovesi R (2005b) Vibration frequencies of $Mg_3Al_2Si_3O_{12}$ pyrope. An ab initio study with the CRYSTAL code. J Phys Chem B 109:6146

Patterson CH (2008) Small polarons and magnetic antiphase boundaries in $Ca_{2-x}Na_xCuO_2Cl_2$ $(x = 0.06, 0.12)$: Origin of striped phases in cuprates. Phys Rev B 77:094523

Prencipe M, Pascale F, Zicovich Wilson CM, Saunders VR, Orlando R, Dovesi R (2004) The vibrational spectrum of calcite ($CaCO_3$): an ab initio quantum-mechanical calculation. Phys Chem Miner 31:559

Rickwood PC, Mathias M, Siebert JC (1968) A study of garnets from eclogite and peridotite xenoliths found in kimberlite. Contrib Mineral Petr 19:271

Rossman GR, Aines RD (1986) Spectroscopy of a birefringent grossular from Asbestos, Quebec, Canada. Am Mineral 71:779

Shanno DF (1970) Conditioning of Quasi-Newton Methods for Function Minimization. Math Comput 24:647

Shtukenberg AG, Yu O Punin, Frank Kamenetskaya OV, Kovalev OG, Sokolov PB (2001) On the origin of anomalous birefringence in grandite garnets. Mineral Mag 65:445

Shtukenberg AG, Popov DYu, Punin YuO (2002) An application of the point-dipole model to the problem of optical anomalies in grandite garnets. Mineral Mag 66:275

Springborg M, Kirtman B (2007) Efficient vector potential method for calculating electronic and nuclear response of infinite periodic systems to finite electric fields. J Chem Phys 126:104107

Takeuchi Y, Haga N, Shigemoto U, Sato G (1982) The derivative structure of silicate garnets in grandite. Z Kristallogr 158:53

Wildner M, Andrut M (2001) The crystal chemistry of birefringent natural uvarovites. Part II. Single-crystal X-ray structures. Am Mineral 86:1231

Zicovich Wilson CM, Pascale F, Roetti C, Saunders VR, Orlando R, Dovesi R (2004) Calculation of the vibration frequencies of α-quartz: the effect of Hamiltonian and basis set. J Comput Chem 25:1873

Zicovich Wilson CM, Torres FJ, Pascale F, Valenzano L, Orlando R, Dovesi R (2008) Ab initio simulation of the IR spectra of pyrope, grossular, and andradite. J Comput Chem 29:2268